ACS OMEGA

http://pubs.acs.org/journal/acsodf

Article

Pt Nanoparticles Confined by Zirconium Metal−Organic Frameworks with Enhanced Enzyme-like Activity for Glucose Detection

Hanhan Wang,[‖] Jun Zhao,[‖] Chuang Liu, Yuping Tong,* and Weiwei He*

Cite This: *ACS Omega* 2021, 6, 4807−4815

Read Online

ACCESS | Metrics & More | Article Recommendations | Supporting Information

ABSTRACT: Metal nanozymes hold promise for chemical and biological applications, and their implementation relies on high catalytic efficiency and stability. Using the metal−organic framework as an ideal carrier for well-dispersed ultra-small metal nanoparticles (NPs) is beneficial for improving the catalytic efficiency of nanozymes. In this study, a zirconium-based metal organic framework (UiO-66) with good chemical stability and high porosity was synthesized and used to construct Pt/UiO-66 nanocomposites. The percentage of Pt in UiO-66 can be tuned easily by adjusting the feeding amount of $PtCl_4^{2-}$. Because of the confinement effect of mesopores, the Pt particles with an average diameter of 3.8 nm are formed and dispersed throughout the pores of the UiO-66 particle. The Pt/UiO-66 composites show efficient oxidase- and peroxidase-like activity. Both the oxidase- and peroxidase-like activities are dependent on the Pt percentage. Pt/UiO-66-6% exhibits enhanced peroxidase-like activity, ∼3.9 times higher than that of commercial Pt/C with 10 wt % Pt. We propose that the construction of Pt/UiO-66 increased the utilization efficiency and stability of Pt NPs and provided more active sites for catalytic reactions. Using the peroxidase-like activity of Pt/UiO-66, a colorimetric method that can be used for actual blood glucose detection was developed for the specific detection of glucose with a limit of detection of 0.033 mM.

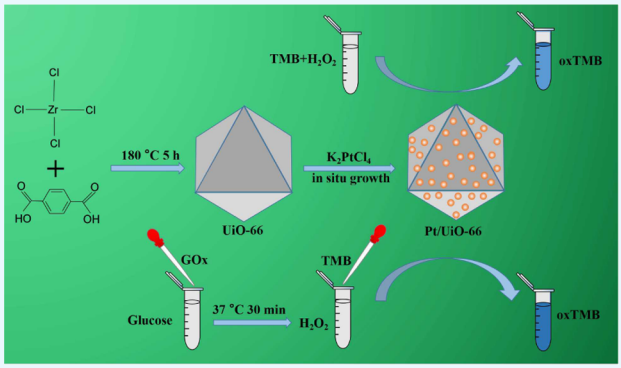

INTRODUCTION

Nanozymes and nanomaterials with enzyme-like activities have been developed as an emerging artificial enzyme to overcome the limitations of natural enzymes, and they have received increasing attention because of their robust stability, ease of preparation, tunable activity, and biomedical applications.[1−6] As a representative, metal nanozymes have the advantages of defined and controllable structures, easy surface modification, good biocompatibility, and multiple enzyme-like activity. In addition, the improvement of enzyme-like activity could be achieved by regulating the size, morphology, surface modification, and composition.[7−12] For example, the glucose oxidase-like activity of Au nanoparticles (NPs) was dependent on their particle size, the catalytic activity decreased with increasing the size of Au NPs from 13 to 50 nm.[12] Especially, benefitting from the advances in catalytic chemistry, metal NPs with a smaller size are expected to increase the catalytic efficiency and utilization efficiency of nanozymes.[13−15] However, NPs usually require surface protection to maintain their stability, while unmodified small particles tend to aggregate, both of which will lead to significant reduction in their catalytic activity.

The loading of small metal NPs on porous carriers has been proven to be an effective way to overcome the above problems to a certain extent.[16,17] Among the porous materials, metal organic frameworks (MOFs) with high porosity, adjustable pore size, large specific surface area, and strong adsorption capacity have attracted extensive attention and is an ideal carrier to support metal NPs.[18−21] In addition, the cavities of MOFs can be used as a template to direct the growth of ultra-small NPs by the confinement effect. For example, Xu's group used the sequential deposition reduction method to load the Au@Ag particle into the pores/surface of ZIF-8, due to the confinement effect of MOF pores, the particle size of the Au@Ag is as small as 2−6 nm and the Au@Ag particle loaded in ZIF-8 exhibited strong catalytic activity toward the reduction of *p*-nitrophenol.[22] Latroche et al. synthesized Pd@MIL-100 by the reduction of H_2PdCl_4 with H_2. The well-distributed Pd

Received: November 25, 2020
Accepted: February 1, 2021
Published: February 11, 2021

Scheme 1. Illustration for the Preparation of the Pt/UiO-66 Hybrid Nanozymes and Detection of Glucose

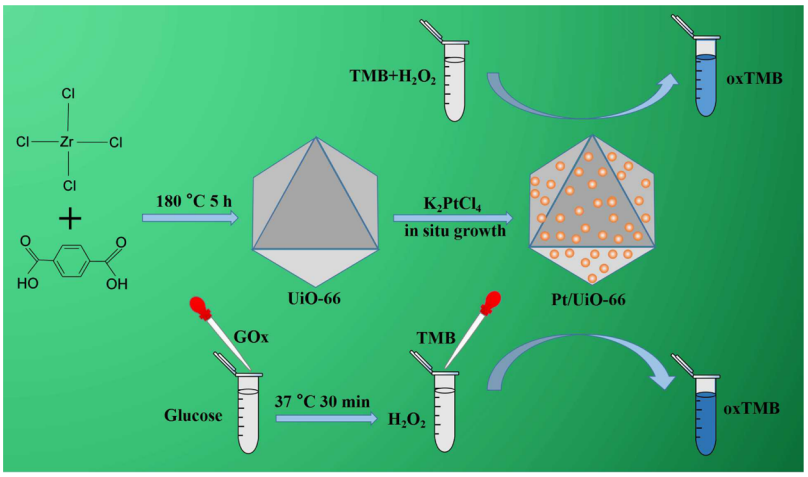

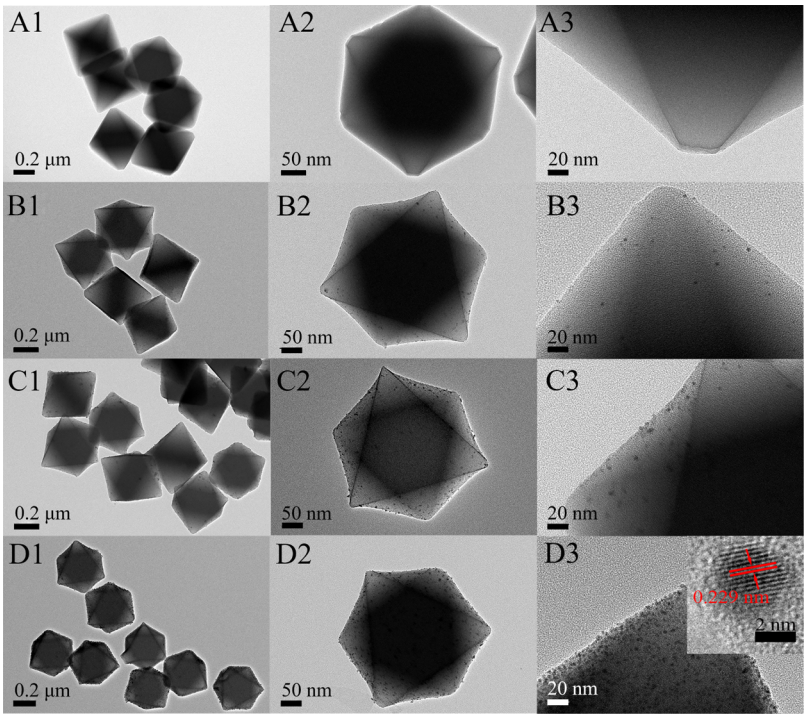

Figure 1. TEM images at low and high magnifications of UiO-66 (A), Pt/UiO-66-1% (B), Pt/UiO-66-3% (C), and Pt/UiO-66-6% (D). The inset in (D3) is HRTEM of the Pt particle.

NPs with an average size of 2.5 nm has greatly improved the storage capacity of H_2.[23] Recently, Gao and co-workers have constructed metalloporphyrinic MOFs decorated with ultra-small Pt NPs, which exhibit high catalytic activity and are used for the electrocatalytic reduction of hydrogen peroxide and oxygen reduction reaction.[24] The MOFs could induce the formation of ultra-small sized particles and prevent their aggregation, resulting in increasing the catalytic activity and stability. The research on the incorporation of nanozymes into MOFs represents an emerging direction. The enzyme-like activity of nanozyme/MOFs composites depends not only on the nature of MOFs but also on the physiochemical state of nanozyme particles (e.g., size, surface, and aggregation). Therefore, there is big space in adjusting the structure and component to optimize the enzyme-like activity.

In this study, zirconium MOFs confined the growth of Pt NPs was explored for enhanced peroxidase-like activity and detection of glucose (Scheme 1). UiO-66, a Zr based MOF, was selected as a nanocarrier because it has additional advantages of high stability against acid/base medium and capability to donor electrons. Octahedral UiO-66 was synthesized by a hydrothermal method and was used to template the reduction of Pt NPs confined by the pores. The prepared Pt/UiO-66 composite maintains a good distribution of Pt ultra-small particles throughout the UiO-66. We investigate the peroxidase-like and oxidase-like activities of the Pt/UiO-66 with different Pt percentages. Compared with the commercial Pt/C catalysts, Pt/UiO-66 exhibits enhanced enzyme-like activity. Using the peroxidase-like activity of Pt/UiO-66, a selective and sensitive colorimetric method for the determination of glucose is established.

https://dx.doi.org/10.1021/acsomega.0c05747
ACS Omega 2021, 6, 4807−4815

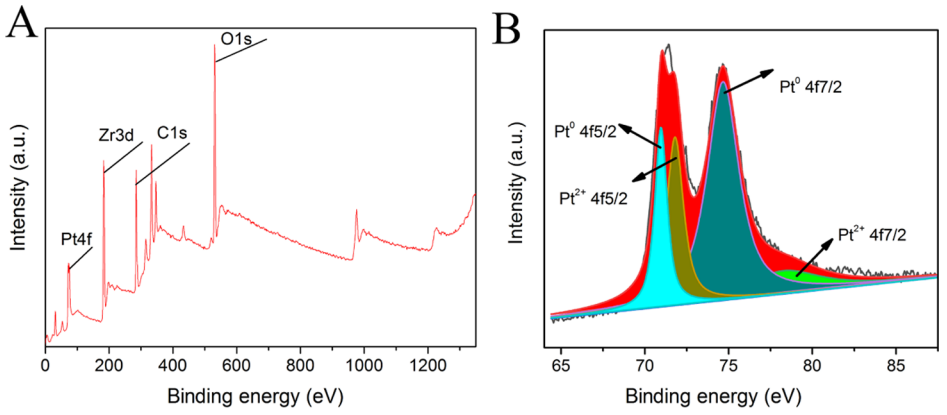

Figure 2. (A) XPS survey of Pt/UiO-66-6% nanocomposites and (B) high-resolution spectra of Pt 4f.

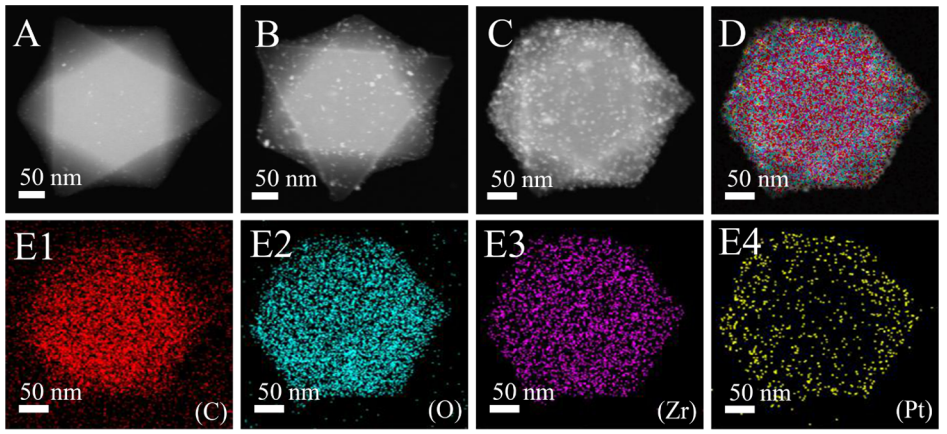

Figure 3. Scanning TEM (STEM)-HAADF image of Pt/UiO-66-1% (A), Pt/UiO-66-3% (B), and Pt/UiO-66-6% (C), and STEM element mapping images of mixed elements (D) and C (E1), O (E2), Zr (E3), and Pt (E4) of Pt/UiO-66-6%, respectively.

RESULTS AND DISCUSSION

The zirconium MOF, UiO-66, was selected as a template to guide the formation of Pt NPs, and it was prepared via the hydrothermal treatment of Zr^{4+} and H_2BDC in *N*,*N*′-dimethylformamide (DMF) solutions. The synthesized UiO-66 are well dispersed and show a uniform octahedral shape with an average diameter of ∼500 nm, a Brunauer−Emmett−Teller (BET) surface area of ∼1327 m^2/g, and average pore size of 3.4 nm (Figures S1A,B and S2). To prepare Pt/UiO-66 nanostructures, the Pt^{2+} ions with the desirable amount were first impregnated into UiO-66 and followed by reduction with fresh $NaBH_4$. A quick color change from white to gray indicates the formation of Pt/UiO-66. Figure 1 shows the transmission electron microscopy (TEM) images of UiO-66 and Pt/UiO-66 with different Pt loading. Compared to the clean structure of pure UiO-66, Pt particles are formed and nearly monodispersed into UiO-66 matrices in Pt/UiO-66 nanocomposites. The density of Pt particles increased gradually with increasing the loading amount of Pt, while the particle size remained unchanged. The inset lattice image of the Pt particle shows that the distance between adjacent lattices is 0.229 nm, corresponding to the planar distance of Pt(111). The X-ray diffraction (XRD) pattern of Pt/UiO-66 shows two additional shoulder signals at 40 and 46°, which corresponds to diffraction peaks of Pt (111) and (200), which is suggestive of the formation of Pt/UiO-66 composites (Figure S3). The X-ray photoelectron spectroscopy (XPS) survey shows the signals from Pt 4f, Zr 3d, C 1s, and O 1s (Figure 2A), confirming again that the elements existed in the Pt/UiO-66 composite. Fitting the high-resolution XPS spectrum of Pt 4f (Figure 2B), the doublet of Pt $4f_{5/2}$ (70.95 eV) and Pt $4f_{7/2}$ (74.65 eV) can be indexed to zero-valent Pt, while the peaks of Pt $4f_{5/2}$ at 71.8 eV and Pt $4f_{7/2}$ at 78.6 eV indicate a small portion of Pt in the oxide state.

The high angle annular dark field (HAADF) images show more clearly that Pt dots are uniformly distributed inside the whole UiO-66 particle (Figure 3A−C). Energy-dispersive X-ray spectroscopy (EDS) analysis confirmed the existence of element Pt and was used to calculate its mass ratio in Pt/UiO-66 (Figure 3D). The measured percentage of Pt is about 0.31 wt % in Pt/UiO-66-1%, 3.07 wt % in Pt/UiO-66-3%, and 5.66 wt % in Pt/UiO-66-6%, respectively (Table S1). This indicates that the added $PtCl_4^{2-}$ was almost completely reduced, thus, we can easily tune the loading percentage of Pt in UiO-66. Taking the Pt/UiO-66-6% as an example, the average diameter of Pt particles is calculated to be ∼3.8 nm, which is matched well with the average pore size of UiO-66. Figure 4 plots both the size distribution of Pt NPs and the pore size distribution (Barrett−Joyner−Halenda equation) of UiO-66, they show the same trend on distribution. The pore size distribution shows that most pores are lower than ∼4 nm in size, which is slightly higher than the average diameter of Pt particles. The TEM images also show that most Pt NPs are incorporated into the voids in UiO-66 (Figure 1). This indicates that the growth of Pt NPs is directed and confined by the pore structure of UiO-66.

https://dx.doi.org/10.1021/acsomega.0c05747
ACS Omega 2021, 6, 4807−4815

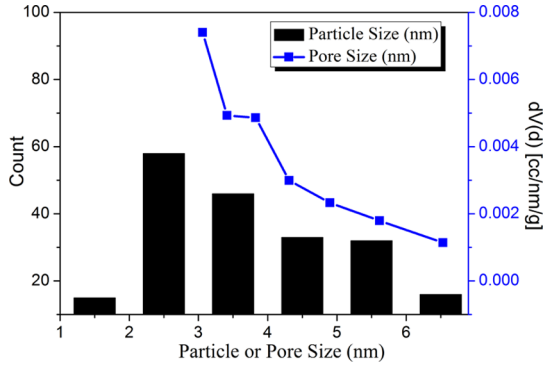

Figure 4. Pore size distribution of UiO-66 and the size distribution of Pt NPs in Pt/UiO-66-6%.

Pt-based NPs have been known to exhibit multiple enzyme-like activities for potential applications in bioassay and therapy. The highly dispersed and small-sized Pt NPs in UiO-66 are beneficial for increasing the enzyme-like activities. To prove this, 3,3′,5,5′-tetramethylbenzidine (TMB) assay was used to investigate the peroxidase- and oxidase-like activities of Pt/UiO-66. Figure 5A compares the TMB oxidation dependence on time in the presence of different catalysts. Pure UiO-66 is inactive to catalyze the oxidation of TMB in the presence of H_2O_2. In contrast, the addition of each Pt/UiO-66 composite can evidently catalyze the oxidation of TMB in the presence of H_2O_2, suggesting their peroxidase-like activity. The peroxidase-like activity of Pt/UiO-66 is linearly dependent on the loading amount of Pt particles (Figure 5A,B). A higher Pt percentage in Pt/UiO-66 results in a higher degree of TMB oxidation, which is indicative of the higher peroxidase-like activity. The commercial Pt/C with 10% Pt was used for comparison. Pt/UiO-66-6% exhibits enhanced peroxidase-like activity, ∼3.9 times higher than that of commercial Pt/C (Figure 5B). In the absence of H_2O_2, Pt/UiO-66 can also catalyze the oxidation TMB accompanied with typically blue products, showing intrinsic oxidase-like activity. The oxidase activity is also dependent on the Pt loading amount (Figure 5C,D). The oxidase-like activity followed the same order as peroxidase-like activity: Pt/UiO-66-6% > Pt/UiO-66-3% > Pt/C (10 wt %) > Pt/UiO-66-1%. The 3 wt % Pt loaded on UiO-66 shows higher enzyme-like catalytic activity than that of 10 wt % Pt on carbon black. This indicated that UiO-66 can serve as an ideal support to increase the utilization efficiency of Pt and provide more active sites for catalytic reactions.

Environmental pH and temperature are the critical factors to affect catalytic activities of natural enzymes and nanozymes. Pt/UiO-66-6% was chosen to investigate the effects of pH and temperature on the peroxidase-like activity (Figure 6). The catalytic activity of Pt/UiO-66-6% showed both pH and temperature-dependent manners. Consistent with other reports, the optimal pH is around 4.0,[25,26] which indicates that acidic conditions are more conducive to TMB oxidation. The catalytic activity decreases obviously by increasing pH over 5.5. TMB has a structure of diamine, which leads to poor solubility in a weak base medium. It was observed that a small amount of precipitation will occur when TMB is added into the buffer solution that is close to neutral and weakly alkaline. This result is consistent with the previous report.[27] To study the effect of temperature, we recorded the absorbance of peaks at 650 and 450 nm, which corresponds to the different

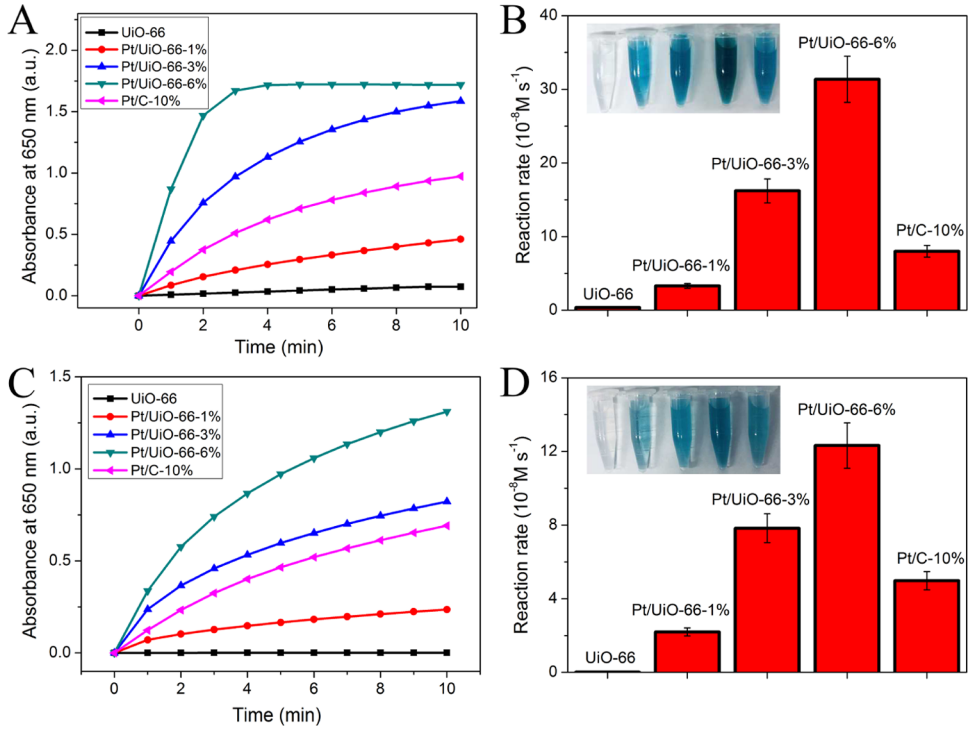

Figure 5. Enzyme-like activity of UiO-66, Pt/UiO-66-1%, Pt/UiO-66-3%, Pt/UiO-66-6%, and commercial Pt/C. (A) Changes in absorbance at 650 nm with time in the solutions containing 0.133 mM TMB, 0.67 mM H_2O_2 and different catalysts. (B) Peroxidase-like activity (reaction rate of TMB oxidation with H_2O_2) of different catalysts, inset shows the photograph of the solution incubated for 3 min. (C) Changes in absorbance at 650 nm with time in the solutions containing 0.133 mM TMB and different catalysts in the absence of H_2O_2. (D) Oxidase-like activity (reaction rate of TMB oxidation) of different catalysts, inset shows the photograph of the solution incubated for 3 min.

https://dx.doi.org/10.1021/acsomega.0c05747
ACS Omega 2021, 6, 4807−4815

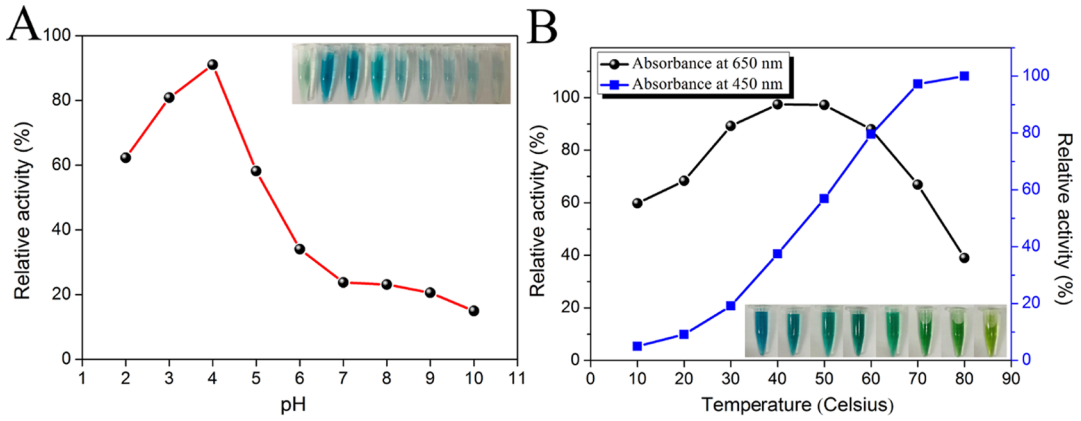

Figure 6. Dependence of the peroxidase-like activity of Pt/UiO-66-6% on the pH (A) and temperature (B). Insets are the photographs of the solution (Pt/UiO-66-6% + TMB + H_2O_2) 3 min under different reaction conditions.

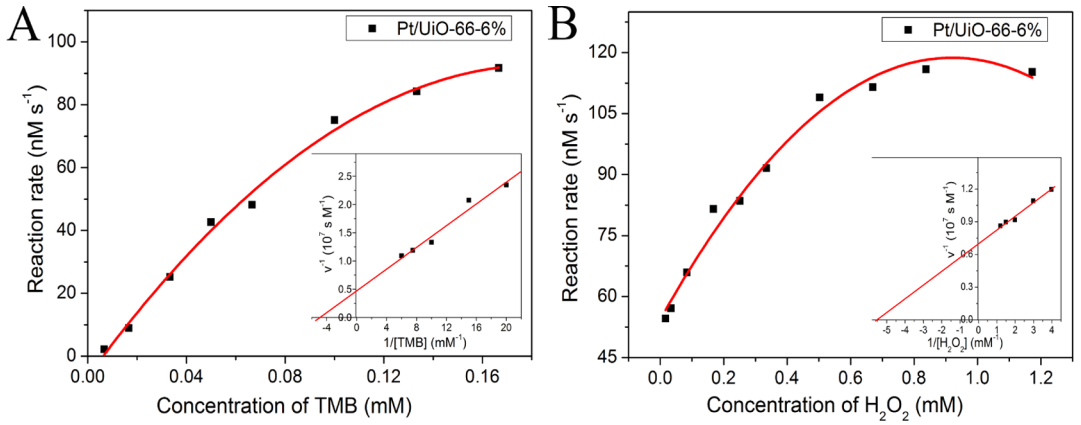

Figure 7. Effect of the concentration of TMB (A) and H_2O_2 (B) on the reaction rate of TMB oxidation catalyzed by Pt/UiO-66-6%. Insets show the corresponding double-reciprocal plots for the calculation of enzyme kinetic parameters by the Michaelis–Menten equation. Conditions: 30 °C in pH 4.5 HAc–NaAc buffer (0.01 M), the concentration of H_2O_2 in (A) is fixed at 0.13 mM, and the concentration of TMB in (B) is fixed at 0.67 mM.

products of TMB oxidation. TMB can be oxidized to produce an intermediate of the blue diamine/diimine charge transfer complex (λ_{max} = 650 nm) or to directly produce the end product of yellow diimine (λ_{max} = 450 nm).[28] It is observed that the catalytic activity calculated from A_{650nm} shows an optimal temperature range from 30 to 60 °C, while the activity calculated from A_{450} increased quasilinearly with temperature. The color of TMB oxidation typically evolved from blue to green and yellow-green, which also verifies the effect of temperature on oxidation products. This indicates that the oxidation of TMB catalyzed by Pt/UiO-66 may go through different ways under low and high temperatures. The blue diamine/diimine complex is the dominant product at temperatures lower than 50 °C, with temperature increasing, the product of yellow diamine becomes dominant. Anyhow, this result demonstrates that pH and temperature-dependent peroxidase-like activity of Pt/UiO-66-6% to oxidize TMB are mainly substrate restricted. Thus, the Pt/UiO-66-6% has a very stable catalytic activity over a wide temperature range.

Pt NPs mimicking peroxidase to oxidize TMB in the presence of hydrogen peroxide was debated in different mechanistic ways. In the interaction between H_2O_2 and Pt NPs, the consumption of hydrogen peroxide assisted by Pt NPs can be through 3 pathways. The reactions 1 and 2 are favorable in accelerating the oxidation of the chromogenic substrate (e.g., TMB and OPD), thus exhibiting enhanced peroxidase-like activity, while the decomposition of H_2O_2 through reaction 3 will slow down the TMB oxidation and inhibit the peroxidase-like activity.

$$H_2O_2 + 2HA \xrightarrow{Pt} 2H_2O + 2A \quad (1)$$

$$H_2O_2 \xrightarrow{Pt} 2^{\bullet}OH \quad (2)$$

$$H_2O_2 \xrightarrow{Pt} H_2O + O_2 \quad (3)$$

Because the dissociation and standard reduction potential of H_2O_2 can be changed by adjusting the pH, the oxidizing/reducing capability of H_2O_2 and its reaction pathway are highly dependent on pH.[29] When pH increases, the standard reduction potential of H_2O_2 decreases and in turn, its oxidizing ability is reduced, reaction 1 slows down. As demonstrated in previous publications,[8,30] when interacting with H_2O_2, Au or Pt NPs can elicit the generation of hydroxyl radicals through pathway 2 at lower pH and the production of dioxygen through pathway 3 at higher pH conditions. This indicates that the pH-dependent peroxidase-like activity of Pt/UiO-66 is not only attributable to the catalytic nature of Pt NPs but also to the pH-dependent physical and chemical properties of the reactant substrates (TMB and H_2O_2).

https://dx.doi.org/10.1021/acsomega.0c05747
ACS Omega 2021, 6, 4807–4815

Table 1. Comparison of K_m, V_{max}, and K_{cat} toward TMB and H_2O_2 for Pt/UiO-66-1%, Pt/UiO-66-3%, Pt/UiO-66-6%, and Commercial Pt/C-10%

catalyst	catalyst concentration [nM]	substrate	K_m [mM]	V_{max} [10^{-8} M s^{-1}]	K_{cat} [s^{-1}]
Pt/UiO-66-1%	0.033	TMB	0.013	1.46	442.42
	0.033	H_2O_2	0.353	1.79	542.42
Pt/UiO-66-3%	0.1	TMB	0.029	3.95	395
	0.1	H_2O_2	0.271	4.73	473
Pt/UiO-66-6%	0.2	TMB	0.204	21.12	1056
	0.2	H_2O_2	0.178	14.23	711.15
Pt/C-10%	0.33	TMB	0.536	13.43	406.97
	0.33	H_2O_2	0.130	5.40	163.64

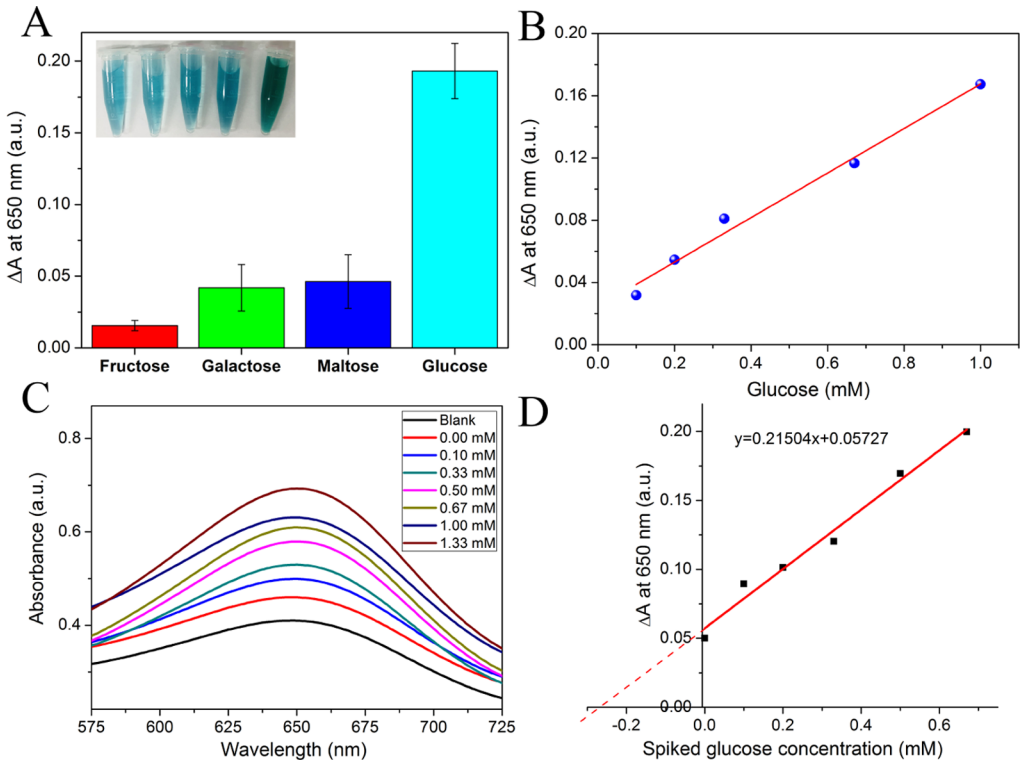

Figure 8. (A) Selectivity of the proposed method for glucose detection, (B) concentration response for glucose detection using Pt/UiO-66-6% as peroxidase mimics. Inset in (A) shows the photographs of TMB after oxidation catalyzed by Pt/UiO-66 in the presence of glucose analogues (from left to right: blank, fructose, galactose, maltose, and glucose), (C) evolution of UV−vis absorption spectra of the blood serum with spiked glucose of different concentrations, (D) standard addition method for the detection of glucose in the serum using Pt/UiO-66-6% as a peroxidase mimic. The dotted line in (D) is the extension of the standard curve in order to calculate the glucose concentration in the unspiked serum sample.

For peroxidase-like activity, the reaction rate was dependent on the reactant concentration (TMB and H_2O_2). Figure 7 shows the effect of the TMB concentration and H_2O_2 concentration on the reaction rate of TMB oxidation. They had a common tendency that the reaction rates gradually increased with TMB or H_2O_2 concentration at lower levels until they reached the maximum. At H_2O_2 concentrations lower than 1.0 mM, a linear relationship in the range from 0.016 to 0.837 mM was found with a limit of detection (LOD) of 5.6 μM (Figure S8). The detection performance of this method is comparable to other enzyme-based and non-enzymatic H_2O_2 detection methods (Table S2). This linear response to hydrogen peroxide can also be applied to detect other biological substances related to H_2O_2 (such as glucose, we will discuss below).

The apparent kinetic parameters of Pt/UiO-66 with different Pt loadings as peroxidase mimetics are determined, as shown in Table 1. The Michaelis−Menten constant (K_m) and the maximal reaction velocity (V_{max}) for the oxidation of TMB were calculated by fitting the typical double-reciprocal plots to Michaelis−Menten mode (inset in Figures 7 and S4−S7). The K_m is the concentration of the substrate [S] when the enzymatic reaction reaches half of the V_{max}. K_m represents the affinity between the enzyme and the substrate. For natural enzymes, a small K_m generally means a high affinity and catalytic activity. It was found that the values of both K_m and V_{max} to substrates TMB and H_2O_2 were highly affected by the Pt percentage in the Pt/UiO-66 composites. With the increase of Pt percentage from 1 to 6%, the K_m and V_{max} for TMB increase gradually. In other words, the Pt/UiO-66 having a higher Pt percentage shows higher K_m and V_{max} values simultaneously. Consistent with the previous publication,[31] these results also indicate that the use of K_m should be critically cautious for evaluating the enzyme-like capabilities of inorganic nanostructures. For H_2O_2, as the Pt percentage increases, K_m gradually decreases, while the V_{max} gradually increases. In a

https://dx.doi.org/10.1021/acsomega.0c05747
ACS Omega 2021, 6, 4807−4815

comprehensive comparison with commercial Pt/C, Pt/UiO-66-6% possesses a lower K_m and higher V_{max} toward both TMB and H_2O_2, suggesting the superior activity of Pt/UiO-66-6% to mimic peroxidase. We compared the apparent kinetic parameters (K_m and V_{max}) of the Pt/UiO-66 nanocomposite as a peroxidase mimic with previous peroxidase-like NPs, as shown in Table S3. Among the catalysts, Pt/UiO-66 showed the highest V_{max} value for TMB.

Many biomolecules produce H_2O_2 after an oxidation reaction. For example, glucose is oxidized in the presence of glucose oxidase to produce gluconic acid and H_2O_2. The peroxidase-like activity of the nanozyme was often used to detect some biologically active molecules involved with H_2O_2. Here, glucose was detected by using the Pt/UiO-66 nanozyme coupled with glucose oxidase. In order to verify the specificity of colorimetric detection of glucose, we conducted control experiments using glucose analogues, such as galactose, fructose, and maltose, at concentrations five times that of glucose. The results show that the colorimetric method has high specificity for the detection of glucose (Figure 8A). For glucose, the absorbance at 650 nm was found to be dependent on the concentration of glucose; higher concentrations of glucose resulted in higher absorption. We used the absorbance change at 650 nm to build a standard curve of ΔA versus glucose concentration (Figure 8B). The curve showed a good linear relationship (R^2 = 0.9822) in the glucose concentration range of 0.1−1.33 mM with a LOD of 0.033 mM (S/N = 3). In order to test the feasibility of this method in real samples, we further tested the glucose concentration in the human serum. The serum sample is spiked with a series concentration of glucose. The change of absorbance at 650 nm is linearly dependent on the concentration of glucose (Figure 8C,D). The concentration of glucose in original blood is determined by the standard addition method to be 5.32 mM, which is consistent with the value (5.29 mM) measured by a biochemical analyzer in the hospital. These results suggest that Pt/UiO-66 NPs can serve as a nano-peroxidase in the colorimetric detection of glucose in actual samples. It is also possible to determine other H_2O_2-related molecules for in vitro diagnostics and personal health care applications.

CONCLUSIONS

In summary, Pt/UiO-66 with tunable percentages of Pt NPs encapsulated inside UiO-66 was synthesized through impregnation followed by the chemical reduction method. With the support and confinement of a three-dimensional mesoporous structure of UiO-66, Pt NPs with a small size are well distributed inside the cavities of UiO-66. Pt/UiO-66 nanocomposites exhibit highly efficient peroxidase-like and oxidase-like activity and are dependent on the Pt percentage. The Pt/UiO-66 with 6 wt % Pt loading show higher enzyme-like catalytic activity, ∼3.9 times higher than that of commercial Pt/C with 10 wt % Pt. In addition, Pt/UiO-66 as enzyme mimetics exhibit excellent catalytic stability against a higher temperature and harsh acid-base environment. Based on the peroxidase-like activity of Pt/UiO-66, a platform for the detection of hydrogen peroxide and glucose has been developed. The formation of the Pt/UiO-66 structure not only can improve the utilization efficiency and stability of Pt NPs but also can provide a more active surface for catalytic reactions. These results also suggest an effective approach to maximize the catalytic efficiency of both nanozyme and natural enzymes in related applications.

EXPERIMENTAL SECTION

Chemicals and Materials. Zirconium tetrachloride ($ZrCl_4$), 1,4-benzenedicarboxylic acid (H_2BDC), DMF, acetic acid, absolute ethanol, potassium tetrachloroplatinate(II) (K_2PtCl_4), sodium borohydride ($NaHB_4$), TMB, and hydrogen peroxide (H_2O_2) were analytically purified and purchased from Sinopharm Chemical Reagent Co., Ltd. (Beijing, China) and glucose oxidase (from *Aspergillus niger*, GOx) were commercially available from Aladdin Industrial Co. (CA, USA). Milli-Q water (18 MΩ cm) was used for all the experimental preparations. All glassware and autoclaves used in the following procedures were cleaned by aqua regia solution (HNO_3/HCl = 1:3 v/v).

Synthesis of Pt/UiO-66 Nanocomposites. First, UiO-66 was synthesized according to the previous method with some modifications.[32] Typically, 116.6 mg of $ZrCl_4$ (0.5 mmol) and 83.1 mg of H_2BDC (0.5 mmol) were each dissolved in 10 mL of DMF and then mixed with the following addition of 4 mL acetic acid. The solution was stirred magnetically for 20 min at room temperature and then transferred to a 50 mL stainless-steel autoclave lined with Teflon, sealed, and placed in an oven at 180 °C for 5 h. After cooling to room temperature, the white precipitate was collected and washed by centrifugation, once with DMF and three times with absolute ethanol. UiO-66 was dried in a vacuum cabinet at 60 °C for further use.

Pt/UiO-66 nanostructures with different Pt contents were prepared by an impregnation and followed by chemical reduction. Typically, for producing Pt/UiO-66 with Pt of 1 wt % (denoted Pt/UiO-66-1%), 9.9 mg of UiO-66 was dispersed in 3 mL of absolute ethanol into which 21 μL of 24 mM K_2PtCl_4 aqueous solution was added. After stirring for 6 h, the Pt^{2+}@UiO-66 was centrifuged to remove free $PtCl_4^{2-}$ ions and re-dispersed into 3 mL of absolute ethanol. The reduction of Pt was initiated by the addition of 20 μL of 0.5 M of sodium borohydride at room temperature. After 2 h, the gray precipitate was collected by centrifugation, washed once with ethanol and twice with water, and then diluted to 2 mL with water for further use. The Pt/UiO-66-3% and Pt/UiO-66-6% were prepared using the same procedure with the addition of a varying amount of K_2PtCl_4.

Characterization. Scanning electron microscopy (SEM) images were captured on a FEI nova 450 field-emission electron microscope. XRD patterns were collected by XRD (Bruker D8 Advance diffractometer) using monochromatized Cu Kα radiation (λ = 1.5418 Å). TEM images were captured on a Tecnai G^2 F20 U-TWIN electron microscope with an accelerating voltage of 200 kV. That same microscope was used to perform dark field imaging, EDS mapping, and high-resolution TEM (HRTEM). XPS was conducted using a Thermo ESCALAB 250XI multifunctional imaging electron spectrometer using 150 W Al Kα radiation and base pressure of approximately 3×10^{-9} mbar. The binding energies were calibrated to the C 1s line at 284.8 eV. UV−visible absorption spectra were obtained by a UV−vis−NIR spectrometer (Varian Cary 5000).

Measurement of Peroxidase-like and Oxidase-like Activities. The peroxidase-like and oxidase-like activities of the Pt/UiO-66 nanostructures were studied by catalyzing the oxidation of TMB in the presence and presence of H_2O_2. First, 20 μL of 20 mM TMB and 20 μL of 0.1 M H_2O_2 were mixed in 3 mL of HAc−NaAc buffer (10 mM, pH = 4), then 10 μL of our 10.0 mg/mL UiO-66 or Pt/UiO-66 suspensions was added

https://dx.doi.org/10.1021/acsomega.0c05747
ACS Omega 2021, 6, 4807−4815

to start the oxidation of TMB. The TMB oxidation accompanied with color changes were monitored by using UV−vis absorption spectroscopy. The reaction kinetic for the catalytic oxidation of TMB was analyzed by recording absorption spectra at 2 min intervals using the scanning kinetics mode. The peroxidase-like activity of commercial Pt/C (10 wt %) to catalyze the TMB oxidation was also tested for comparison. The oxidase-like activity of these NPs was accessed by the same procedure, except that hydrogen peroxide was not added.

The apparent steady-state kinetic measurements of dynamics were carried out for different Pt/UiO-66 nanostructures. The parameters were calculated based on the Michaelis−Menten equation

$$1/\nu = (K_m/V_{max}) \times (1/[S]) + 1/V_{max}$$

where ν is the reaction initial velocity, V_{max} is the maximal reaction velocity, [S] is the concentration of the substrate, and K_m is the Michaelis constant. ν is the initial reaction rate.

Detection of Glucose. The peroxidase-like capabilities of Pt/UiO-66 was used to detect glucose. Glucose was first oxidized in the presence of glucose oxidase to produce gluconic acid and H_2O_2 in a pH 7.4 buffer solution; then, we used the TMB assay to detect the concentration of H_2O_2 accelerated by Pt/UiO-66 NPs. Typically, glucose oxidase (40 μL, 100 U mL^{-1}) and glucose aqueous solution (480 μL) with different concentrations were incubated at 37 °C for 30 min. Then, 2.5 mL of HAc−NaAc (10 mM, pH = 4.0) buffer containing 20 mM TMB were added. A portion of the Pt/UiO-66 suspension (20 μL, 33 μg mL^{-1}) was added to trigger the color-change reaction. The mixture was incubated at 37 °C for 4 min, followed by recording the UV−vis absorption spectra. To determine the selectivity of this method for glucose detection, we also ran experiments using other sugars instead of glucose, such as maltose (1 mM), galactose (1 mM), and fructose (1 mM), and other conditions remained unchanged. For testing the applicability of this method to a real sample, the human blood serum from the School of Medicine at Xuchang University was used as received and diluted 20-fold. A standard addition method was used to detect the glucose in the serum. Serum samples were spiked with 0, 0.10, 0.20, 0.33, 0.67, 1.00, and 1.33 mM glucose, respectively. Then, the unspiked and spiked serum samples were treated by the same procedure as that described above to setup the standard curve for the detection of glucose.

■ ASSOCIATED CONTENT

Supporting Information

The Supporting Information is available free of charge at https://pubs.acs.org/doi/10.1021/acsomega.0c05747.

Additional SEM image, N_2 adsorption−desorption isotherm, XRD patterns, calculation of enzyme kinetic parameters, concentration response for H_2O_2 detection, comparison of the performance of various hydrogen peroxide sensors, measured element content of Pt/UiO-66-1%, Pt/UiO-66-3%, and Pt/UiO-66-6% by EDS analysis, comparison of the performance of various hydrogen peroxide sensors, and comparison of *Km* and *Vmax* among the peroxidase-like nanozymes. (PDF)

■ AUTHOR INFORMATION

Corresponding Authors

Yuping Tong − *School of Civil Engineering and Communication, North China University of Water Resources and Electric Power, Zhengzhou, Henan 450045, China*; Email: yptong_zz@163.com

Weiwei He − *Key Laboratory of Micro-Nano Materials for Energy Storage and Conversion of Henan Province, Institute of Surface Micro and Nano Materials, College of Chemical and Materials Engineering and Henan Joint International Research Laboratory of Nanomaterials for Energy and Catalysis, Xuchang University, Xuchang, Henan 461000, P. R. China*; orcid.org/0000-0002-3495-9514; Email: heweiweixcu@gmail.com

Authors

Hanhan Wang − *Key Laboratory of Micro-Nano Materials for Energy Storage and Conversion of Henan Province, Institute of Surface Micro and Nano Materials, College of Chemical and Materials Engineering, Xuchang University, Xuchang, Henan 461000, P. R. China; School of Civil Engineering and Communication, North China University of Water Resources and Electric Power, Zhengzhou, Henan 450045, China*

Jun Zhao − *Key Laboratory of Micro-Nano Materials for Energy Storage and Conversion of Henan Province, Institute of Surface Micro and Nano Materials, College of Chemical and Materials Engineering, Xuchang University, Xuchang, Henan 461000, P. R. China; School of Civil Engineering and Communication, North China University of Water Resources and Electric Power, Zhengzhou, Henan 450045, China*

Chuang Liu − *Key Laboratory of Micro-Nano Materials for Energy Storage and Conversion of Henan Province, Institute of Surface Micro and Nano Materials, College of Chemical and Materials Engineering, Xuchang University, Xuchang, Henan 461000, P. R. China*

Complete contact information is available at: https://pubs.acs.org/10.1021/acsomega.0c05747

Author Contributions

‖H.W. and J.Z. contributed equally to this work.

Notes

The authors declare no competing financial interest.

■ ACKNOWLEDGMENTS

We thank Dr. Hongfang Guo from School of Medicine at Xuchang University for her assistance with blood glucose analysis. This work is supported financially by the National Natural Science Foundation of China (51772256 and 21805085), the Program for Innovative Research Team (in Science and Technology) in University of Henan Province (19IRTSTHN026) and the Program for Zhongyuan Leading Talents of Science and Technology Innovation in Henan Province (204200510016).

■ REFERENCES

(1) Wu, J.; Wang, X.; Wang, Q.; Lou, Z.; Li, S.; Zhu, Y.; Qin, L.; Wei, H. Nanomaterials with Enzyme-like Characteristics (nanozymes): Next-generation Artificial Enzymes (II). *Chem. Soc. Rev.* **2019**, *48*, 1004−1076.

(2) Jiang, D.; Ni, D.; Rosenkrans, Z. T.; Huang, P.; Yan, X.; Cai, W. Nanozyme: New Horizons for Responsive Biomedical Applications. *Chem. Soc. Rev.* **2019**, *48*, 3683−3704.

(3) Huang, Y.; Ren, J.; Qu, X. Nanozymes: Classification, Catalytic Mechanisms, Activity Regulation, and Applications. *Chem. Rev.* **2019**, *119*, 4357−4412.
(4) He, W.; Wamer, W.; Xia, Q.; Yin, J.-J.; Fu, P. P. Enzyme-like Activity of Nanomaterials. *J. Environ. Sci. Health, Part C: Environ. Carcinog. Ecotoxicol. Rev.* **2014**, *32*, 186−211.
(5) Dong, H.; Fan, Y.; Zhang, W.; Gu, N.; Zhang, Y. Catalytic Mechanisms of Nanozymes and Their Applications in Biomedicine. *Bioconjugate Chem.* **2019**, *30*, 1273−1296.
(6) Moglianetti, M.; De Luca, E.; Pedone, D.; Marotta, R.; Catelani, T.; Sartori, B.; Amenitsch, H.; Retta, S. F.; Pompa, P. P. Platinum Nanozymes Recover Cellular ROS Homeostasis in an Oxidative Stress-mediated Disease Model. *Nanoscale* **2016**, *8*, 3739−3752.
(7) Zhou, Y.-T.; He, W.; Wamer, W. G.; Hu, X.; Wu, X.; Lo, Y. M.; Yin, J.-J. Enzyme-mimetic Effects of Gold@platinum Nanorods on the Antioxidant Activity of Ascorbic Acid. *Nanoscale* **2013**, *5*, 1583−1591.
(8) He, W.; Zhou, Y.-T.; Wamer, W. G.; Hu, X.; Wu, X.; Zheng, Z.; Boudreau, M. D.; Yin, J.-J. Intrinsic Catalytic Activity of Au Nanoparticles with Respect to Hydrogen Peroxide Decomposition and Superoxide Scavenging. *Biomaterials* **2013**, *34*, 765−773.
(9) He, W.; Wu, X.; Liu, J.; Hu, X.; Zhang, K.; Hou, S.; Zhou, W.; Xie, S. Design of AgM Bimetallic Alloy Nanostructures (M = Au, Pd, Pt) with Tunable Morphology and Peroxidase-like Activity. *Chem. Mater.* **2010**, *22*, 2988−2994.
(10) Jv, Y.; Li, B.; Cao, R. Positively-charged Gold Nanoparticles as Peroxidiase Mimic and Their Application in Hydrogen Peroxide and Glucose Detection. *Chem. Commun.* **2010**, *46*, 8017−8019.
(11) Ge, C.; Fang, G.; Shen, X.; Chong, Y.; Wamer, W. G.; Gao, X.; Chai, Z.; Chen, C.; Yin, J.-J. Facet Energy Versus Enzyme-like Activities: the Unexpected Protection of Palladium Nanocrystals Against Oxidative Damage. *ACS Nano* **2016**, *10*, 10436−10445.
(12) Luo, W.; Zhu, C.; Su, S.; Li, D.; He, Y.; Huang, Q.; Fan, C. Self-catalyzed, Self-limiting Growth of Glucose Oxidase-mimicking Gold Nanoparticles. *ACS Nano* **2010**, *4*, 7451−7458.
(13) Xiang, H.; Feng, W.; Chen, Y. Single-atom Catalysts in Catalytic Biomedicine. *Adv. Mater.* **2020**, *32*, 1905994.
(14) Zhang, H.; Lu, X. F.; Wu, Z.-P.; Lou, X. W. D. Emerging Multifunctional Single-atom Catalysts/nanozymes. *ACS Cent. Sci.* **2020**, *6*, 1288−1301.
(15) Wang, M.; Liu, L.; Xie, X.; Zhou, X.; Lin, Z.; Su, X. Single-atom Iron Containing Nanozyme with Peroxidase-like Activity and Copper Nanoclusters Based Ratio Fluorescent Strategy for Acetylcholinesterase Activity Sensing. *Sens. Actuators, B* **2020**, *313*, 128023.
(16) Liu, Y.; Tsunoyama, H.; Akita, T.; Xie, S.; Tsukuda, T. Aerobic Oxidation of Cyclohexane Catalyzed by Size-Controlled Au Clusters on Hydroxyapatite:Size Effect in the Sub-2 nm Regime. *ACS Catal.* **2010**, *1*, 2−6.
(17) Yoskamtorn, T.; Yamazoe, S.; Takahata, R.; Nishigaki, J.-i.; Thivasasith, A.; Limtrakul, J.; Tsukuda, T. Thiolate-Mediated Selectivity Control in Aerobic Alcohol Oxidation by Porous Carbon-Supported Au Clusters. *ACS Catal.* **2014**, *4*, 3696−3700.
(18) Liang, S.; Wu, X.-L.; Xiong, J.; Zong, M.-H.; Lou, W.-Y. Metal-organic Frameworks as Novel Matrices for Efficient Enzyme Immobilization: an Update Review. *Coord. Chem. Rev.* **2020**, *406*, 213149.
(19) Wu, T.; Ma, Z.; Li, P.; Lu, Q.; Liu, M.; Li, H.; Zhang, Y.; Yao, S. Bifunctional Colorimetric Biosensors Via Regulation of the Dual Nanoenzyme Activity of Carbonized FeCo-ZIF. *Sens. Actuators, B* **2019**, *290*, 357−363.
(20) Hu, W. C.; Younis, M. R.; Zhou, Y.; Wang, C.; Xia, X. H. In Situ Fabrication of Ultrasmall Gold Nanoparticles/2D MOFs Hybrid as Nanozyme for Antibacterial Therapy. *Small* **2020**, *16*, 2000553.
(21) Hu, P.; Morabito, J. V.; Tsung, C.-K. Core-shell Catalysts of Metal Nanoparticle Core and Metal-organic Framework Shell. *ACS Catal.* **2014**, *4*, 4409−4419.
(22) Jiang, H.-L.; Akita, T.; Ishida, T.; Haruta, M.; Xu, Q. Synergistic Catalysis of Au@Ag Core-shell Nanoparticles Stabilized on Metal-organic Framework. *J. Am. Chem. Soc.* **2011**, *133*, 1304−1306.
(23) Zlotea, C.; Campesi, R.; Cuevas, F.; Leroy, E.; Dibandjo, P.; Volkringer, C.; Loiseau, T.; Fére, G.; Latroche, M. Pd Nanoparticles Embedded into a Metal-organic Framework: Synthesis, Structural Characteristics, and Hydrogen Sorption Properties. *J. Am. Chem. Soc.* **2010**, *132*, 2991−2997.
(24) Ling, P.; Cheng, S.; Chen, N.; Qian, C.; Gao, F. Nanozyme-modified Metal-organic Frameworks with Multienzymes Activity as Biomimetic Catalysts and Electrocatalytic Interfaces. *ACS Appl. Mater. Interfaces* **2020**, *12*, 17185−17192.
(25) Ray, S.; Biswas, R.; Banerjee, R.; Biswas, P. A Gold Nanoparticle-intercalated Mesoporous Silica-based Nanozyme for the Selective Colorimetric Detection of Dopamine. *Nanoscale Adv.* **2020**, *2*, 734−745.
(26) He, W.; Cai, J.; Zhang, H.; Zhang, L.; Zhang, X.; Li, J.; Yin, J.-J. Formation of PtCuCo Trimetallic Nanostructures with Enhanced Catalytic and Enzyme-like Activities for Biodetection. *ACS Appl. Nano Mater.* **2018**, *1*, 222−231.
(27) He, W.; Liu, Y.; Yuan, J.; Yin, J.-J.; Wu, X.; Hu, X.; Zhang, K.; Liu, J.; Chen, C.; Ji, Y.; Guo, Y. Au@Pt Nanostructures as Oxidase and Peroxidase Mimetics for Use in Immunoassays. *Biomaterials* **2011**, *32*, 1139−1147.
(28) Dalui, A.; Pradhan, B.; Thupakula, U.; Khan, A. H.; Kumar, G. S.; Ghosh, T.; Satpati, B.; Acharya, S. Insight Into the Mechanism Revealing the Peroxidase Mimetic Catalytic Activity of Quaternary CuZnFeS Nanocrystals: Colorimetric Biosensing of Hydrogen Peroxide and Glucose. *Nanoscale* **2015**, *7*, 9062−9074.
(29) Rabai, G.; Kustin, K.; Epstein, I. R. A Systematically Designed pH Oscillator: the Hydrogen Peroxide-sulfite-ferrocyanide Reaction in a Continuous-flow Stirred Tank Reactor. *J. Am. Chem. Soc.* **1989**, *111*, 3870−3874.
(30) Liu, Y.; Wu, H.; Li, M.; Yin, J.-J.; Nie, Z. pH Dependent Catalytic Activities of Platinum Nanoparticles with Respect to the Decomposition of Hydrogen Peroxide and Scavenging of Superoxide and Singlet Oxygen. *Nanoscale* **2014**, *6*, 11904−11910.
(31) He, W.; Han, X.; Jia, H.; Cai, J.; Zhou, Y.; Zheng, Z. AuPt Alloy Nanostructures with Tunable Composition and Enzyme-like Activities for Colorimetric Detection of Bisulfide. *Sci. Rep.* **2017**, *7*, 40103.
(32) Sha, Z.; Wu, J. Enhanced Visible-light Photocatalytic Performance of BiOBr/UiO-66(Zr) Composite for Dye Degradation with the Assistance of UiO-66. *RSC Adv.* **2015**, *5*, 39592−39600.

https://dx.doi.org/10.1021/acsomega.0c05747
ACS Omega 2021, 6, 4807−4815